Journal Name

ARTICLE

Au Nanorod Plasmonic Superstructures Obtained by a Combined Droplet Evaporation and Stamping Method

Carola Schopf, Alfonso Martín, Mícheál Burke, Daniel Jones, Andrea Pescaglini, Alan O'Riordan and Aidan J. Quinn and Daniela Iacopino[a]

A combined droplet evaporation and stamping method is presented for the fabrication of Au nanorod superstructures. Specifically, domains of nanorods parallel to the substrate in a close-packed side-to-side fashion are obtained by evaporation of Au chlorobenzene solutions, followed by stamping of the dried droplet on transparent substrates. To understand and optimize the assembly mechanism, synthetic parameters affecting the droplet evaporation process are carefully investigated. Optical characterization of individual domains show markedly anisotropic extinction, confirming the high degree of internal order generated by aligned nanorods. In addition, the unique orientation of domains produces unique distribution of color intensities, which are used for initial demonstration of a novel plasmonic encoding/decoding system.

Introduction

Au nanorods possess unusual optical properties desirable for a number of applications ranging from photonic to sensing.[1-3] The dimensional anisotropy of Au nanorods results in strong polarization-dependent surface-plasmon-based optical properties. Therefore, Au nanorod assemblies constitute ideal candidates for the preparation of optically anisotropic superstructures that allow manipulation of light in the nanoscale.[4,5] Moreover, enhanced optical phenomena taking place in nanorod assemblies can be applied in fields such as sensing, negative refractive index metamaterials or information technologies.[6-9]

In order to further exploit this potential, great efforts have been devoted to the development of suitable techniques to organize Au nanorods into designed assemblies, such as template methods,[10,11] drying at an interface,[12] association in solution,[13] capillary assembly[14] and chemical modification of nanorod surfaces.[15,16] However, most of these processes have led to the formation of structures limited in size to few microns and with poorly defined shapes and inhomogeneous thicknesses.

Recently, droplet deposition has emerged as a promising technique to organize metal nanorods into two- and three-dimensional (2D and 3D) superstructures.[17-19] Using this method Wang et al. have observed formation of nematic and smectic superstructures 15–50 μm in width and 1.7–2.2 μm in depth formed from evaporation of aqueous droplets.[20] At present, a key challenge in the implementation of such structures for practical applications is the limited availability of processes for the fabrication of larger size assemblies, with homogeneous thickness and highly controlled geometrical order. Toward this end, relatively large area ordered arrays have recently been obtained by applying finer control on parameters regulating the droplet evaporation assembly

process. For example controlled evaporation rates were used by Xie et al. to obtain vertically oriented nanorod domains up to 100 μm² in size.[21] Also, Xiong et al. used evaporation of controlled ionic strength droplets to obtain vertically oriented nanorod monolayers which were used for SERS detection of food contaminants.[22]

In this paper we use a droplet evaporation and stamping method to fabricate parallel Au nanorod monolayer assemblies of 200 μm² size on average. Controlled droplet evaporation of nanorod chlorobenzene solutions led to the formation of domains of nanorods assembled parallel to the substrate in a close-packed side-by-side fashion. The obtained assemblies were subsequently stamped intact on transparent substrates, resulting in the formation of homogeneous and chemically robust ordered structures. Optical measurements on individual domains revealed markedly anisotropic extinction, confirming the high degree of internal order generated by aligned nanorods. Domain ensembles showed unique optical characteristics resulting in unique color distributions, which constitute the basic idea for the development of a novel plasmonic encoding/decoding system. As proof-of-concept, conversion of three optically polarized transmission images into unique histograms is presented, together with a representative QR code generated from one of the areas.

Experimental

Synthesis. Au nanorods (AR = 3.6) were synthesized by the seed-mediated method reported by El Sayed et al.[23] Au nanorods with AR = 4, 3 and 2 were obtained by modifications of the seed-mediated method described in details in the SI. As-prepared Au nanorods were centrifuged and redispersed into water, in order to maintain a CTAB concentration between 0.01 and 0.2 mM. Au nanorods in water solutions were transferred in chlorobenzene following the method described by Chen.[24]

Fabrication of ordered Au nanorod superstructures. A small aliquot (10 µL) of Au nanorod cholobenzene solution ([Au] = 2-10 nM) was deposited on SiO_2 substrate, covered with a petri dish and then left to evaporate at room temperature over a time of 3 h. Controlled solvent evaporation resulted in formation of parallel assemblies. Fabricated assemblies were transferred intact onto transparent supports by placing a glass coverslip on the original SiO_2 substrate and pressing the two surfaces together for 30 s. Excess organic matter was removed by immersing glass-nanorod assemblies in isopropanol for 1 h, followed by multiple rinses with fresh isopropanol. The process is described in more details elsewhere.[25]

Electron Microscopy. Scanning electron microscopy (SEM) images of nanorod solutions and nanorod 2D lattices were acquired using a field emission SEM (JSM-6700F, JEOL UK Ltd.) operating at beam voltages of 2 kV.

Alignment marks were made using a Quanta 3D 200i dual-beam Focused Ion Beam (FIB). Individual 4 µm × 1 µm rectangles were fabricated on the sample by focused ion beam milling; 30 kV beam voltage, 100 pA beam current, a depth of 100 nm. These individual rectangles were arranged to form the marks shown in Figure 4. Two of these rectangles (one horizontal, one vertical) form the 'L' shape at each corner.

Optical characterization. Polarized optical images and transmission spectra of gold nanorod superstructures were acquired with an inverted IX-71 Olympus microscope with a 100X objective. The sample was illuminated with a 100 W halogen lamp. The light collected by the objective was directed either unto a color CMOS camera (DCC1645C, ThorLabs) for image acquisition or into the entrance of slit of a monochromator (SP-300i, Acton Research) equipped with a thermoelectrically cooled, back illuminated CCD (Spec10:100B, Princeton Instruments) for spectra acquisition. The sample polarization rate was determined by a polarizer placed between the lamp and the sample. Spectra were typically recorded using an integration time of 1-10 s. The extinction was determined according to Lambert-Beer's law: A= $-\log_{10}(I/I_0)$ with I being the sample spectrum and I0 being the blank spectrum taken from a nearby clean area on the substrate.

Results and discussion

Au nanorods were synthesized by a standard seed-mediated method described by El Sayed *et al.*[23] The as-prepared Au nanorod solution (1 mL) was centrifuged twice to remove cetyltrimetylammonium bromide (CTAB) excess and re-dispersed in 1 mL of Millipore water. The final CTAB concentration was kept between 0.01 and 0.2 mM. The nanorods' mean diameter and length were 11 ± 2 nm and 40 ± 3 nm respectively, aspect ratio (AR) = 3.6. Prior to deposition on solid substrates, nanorods were transferred into chlorobenzene following the method described by Chen *et al.*[24]

Figure 1a shows a low magnification SEM image of ordered superstructures formed by droplet deposition of Au nanorod chlorobenzene solutions (10 µl, 10 nM) onto SiO_2 substrates. Under slow (3 h) and controlled evaporation conditions, nanorods assembled into domains of average size 200 µm², covering the entire area of a 5 mm diameter droplet. SEM images of an individual domain (Figure 1b) revealed the formation of a solid Au nanorod monolayer phase, ordered both orientationally and positionally. Fast Fourier transform analysis shown in the inset of Figure 1b displays diffuse streaks corresponding to side-by-side alignment of nanorods, confirming a high degree of ordering. Evidence of monolayer

formation is shown in Figure 1c depicting a 45° tilted SEM image of the superstructure.

Formed assemblies were subsequently stamped on glass coverslips. This step allowed the efficient removal of excess organic surfactant and resulted in improved adhesion of the assemblies on substrates. Figure 1d shows a SEM image of parallel assemblies obtained using this stamping method whereby both the packing configuration and ordering of the nanorods is shown to be maintained.
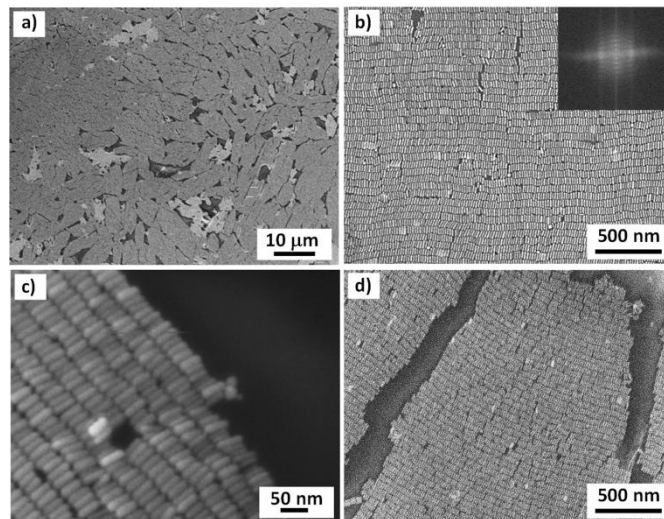

Figure 1. SEM images of Au nanorod superstructures; a) domains obtained by droplet evaporation of nanorod chlorobenzene solutions on SiO_2; b) high magnification image showing parallel alignment of Au nanorods within an individual domain. Inset: Fast Fourier Transform of the image shown in b); c) 45° tilted image of a nanorod domain showing evidence of monolayer formation; d) image of nanorod domains stamped on glass coverslip substrates.

In order to gain a deeper understanding of the mechanism regulating the formation of Au superstructures during droplet evaporation, investigation of the effects played by the following parameters was undertaken: nanorod solution concentration, surfactant concentration, substrate, evaporation rate, nanorod aspect ratio and solvent.

Ordered assemblies formed across a relatively large range of Au nanorod concentrations, between 0.1 nM and 10 nM. The domain size was found to be dependent on the initial concentration of the nanorod solution. In particular, at low concentrations nanorods arranged parallel to each other into isolated domains with sizes ranging from 0.2 to 25 µm². At higher nanorod concentrations domain size increased to an average 200 µm². Also, the separation between neighboring domains decreased until, for nanorod concentrations of 10 nM and higher, domains merged covering the entire area of the drop (see Figure SI2). The highest degree of order was obtained for CTAB concentrations between 0.01 and 0.2 mM. Higher CTAB concentrations produced less ordered structures; at lower CTAB concentration nanorods became unstable and did not transfer into organic phase (see Figure SI3). Variation of tetraoctylammoniumbromide (TOAB) concentration from the 50 mM value used for phase transfer did not affect the final degree of order obtained. Regarding the effect of substrates, superstructures of comparable high order were obtained from droplet evaporation on SiO2, glass and glass/ITO substrates (contact angles 52°, 40° and 72° respectively). The evaporation rate was slowed down to 3 h by covering the droplet with a petri dish. Faster evaporation rates < 1 h resulted in disordered assemblies (Figure SI4). The nanorod dimensions did not

affect the assembly process, which produced equally ordered superstructures with nanorods of aspect ratios 2 - 4 (Figure SI5). Finally, the use of the chlorobenzene solvent was essential for the generation of long-range ordering observed in our superstructures. Analogous droplet deposition of Au nanorods from aqueous solutions produced mixed parallel and perpendicular multi-layered superstructures, in agreement with coffee-stain mechanisms (Figure SI6). The compactness and high degree of order obtained from chlorobenzene dispersions was attributed to the lower vapor pressure and lower viscosity of chlorobenzene compared to water. These factors promoted a higher degree of ordering by i) slowing down the evaporation process, thus allowing more nanorods to be at an equilibrium position and assemble together in the solution before droplet evaporation and ii) offering less resistance to domain movement. The assembly into parallel lines has been observed for Au nanorods with surface anchored lipids.[26] Interestingly, droplet evaporation of water solutions resulted in isotropic structures whereas nanorods assembled into 1D configurations when chloroform was used to assist the droplet evaporation process.

Self-assembly occurs when repulsive and attractive interactions among nanorods are balanced. The formation of superstructures was found highly dependent on the critical concentration of the nanorods. As the solvent evaporated, the Au nanorods reached a critical concentration and self-assembled on the three-phase contact line (at the interface between vapor, substrate and solution). According to previous reports,[27] when nanorods are at low supersaturated concentration, contact with the substrate through one plane (side-by-side) is the most favorable way of deposition. The self-assembly process was also found highly dependent on the CTAB concentration. The estimated distance between adjacent nanorods in the dried droplet was ca. 3 nm, suggesting that CTAB molecules from adjacent nanorods were inter-digitated (length of a fully stretched CTA^+ ion is 2.2 nm).[28,29] Therefore CTAB was the glue that held together nanorods and regulated inter-nanorod distances through short range repulsion and steric hindrance of the surfactant chains.[30]

Real time observations of the evaporation process by polarized optical microscopy showed evidence of monolayer islands formation at the interface between solvent and air. The islands grew in size as the droplet evaporated. Formation of multilayers was prevented by the high electrostatic repulsion between the islands. The process is discussed in details in Figure SI7.

In order to explore optical properties, superstructures stamped on glass coverslips were examined by optical transmission imaging and spectroscopy. Optical images of nanorods aligned within domains of an average size of 200 μm^2 were acquired under polarized excitation parallel and perpendicular to the long axes of individual nanorods (Figure 2a). Due to the high degree of internal order, domains changed color from light green to dark green as the polarization direction was oriented parallel or perpendicular to the nanorod long axes. The origin of this colour shift can be explained by the selective excitation of the longitudinal and transversal surface plasmon resonance (SPR) modes of the nanorods, respectively. Figure 2b shows extinction spectra of the domain indicated by an arrow in Figure 2a. The spectrum recorded with un-polarized light was characterized by a broad transversal resonance peak with a max at 650 nm. The max was red-shifted in comparison to the 520 nm value of isolated nanorods, due to plasmon coupling of closely-spaced nanorods within the superstructure. The longitudinal peak was barely detected as shoulder at higher wavelengths. The spectrum measured under polarized light

parallel to the direction of the nanorod long axes (30º, blue curve) showed a selective excitation of the longitudinal plasmon mode, resulting in a peak at 720 nm. The excitation of the transversal plasmon mode (120º, green curve) resulted in a broad spectrum with a peak centered at 641 nm. Both spectra only showed contribution from one mode, and could be fitted by a single Lorentzian function. The longitudinal peak at 720 nm was blue-shifted compared to the absorption peak of isotropic dispersions of the same nanorods at 754 nm.
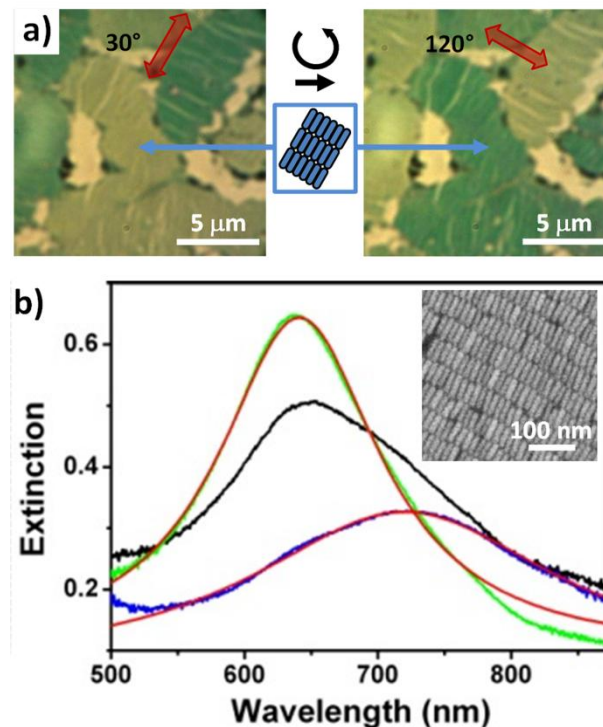

Figure 2. a) Polarized transmission images of Au nanorod domains showing light green to dark green color transition associated to the relative orientation of polarized light with the long axes of nanorods that constitute the domains. b) Extinction spectra of the nanorod domain indicated in a) acquired with non-polarized excitation (black) and with polarized excitation perpendicular (120°, green curve) and parallel (30°, blue curve) to the nanorod longitudinal axes. Red lines are Lorentzian fits to the data. Inset: SEM image showing the ordering of the nanorods within the domain where the spectra were taken.

Simulated extinction spectrum of nanorods organized on a 2x6 array reported in SI8 showed maxima at 540 nm and 720 nm for light polarised in direction perpendicular and parallel to the nanorod long axes, respectively. The array longitudinal mode was blue shifted compared to the simulated value of an individual nanorod (733 nm), in agreement with theoretical studies of parallel assemblies of nanorods, which are known to produce a blue-shift of the SPR band in the UV-vis spectrum.[31] A correlated SEM image of the optically characterized nanorod domain is shown as inset in Figure 2b, confirming the high degree of order of the imaged area constituted by tightly packed nanorods. Polarization-dependent colour changes have been recently reported in literature for individual nanorods imaged by polarised dark-field.[32] Interestingly, the variety of colors at different polarisation angles could only be detected for nanorods with diameters larger than 37 nm, due to the otherwise too small scattering cross section. Accordingly, simulated spectra (SI8) and experimental data, showed that extinction spectra of individual nanorods comprising the superstructures could not be recorded, due to the nanorod small scattering cross section. However, for nanorods assembled in

superstructures strong transversal and longitudinal couplings resulted in the optical features described in Figure 3 (see also experimental and simulated spectra in SI8).
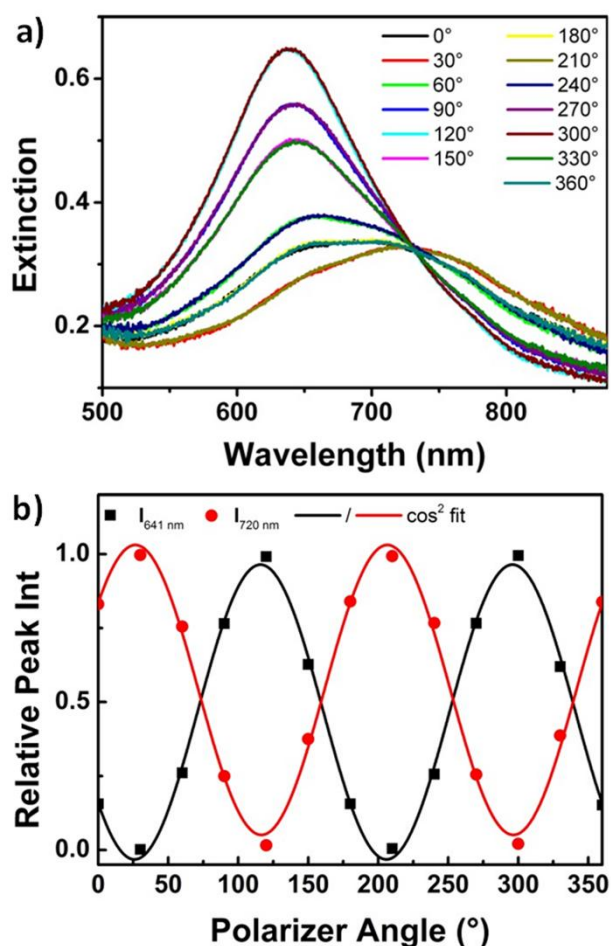

Figure 3. a) Extinction spectra of an individual nanorod domain for varying polarization angles; b) Relative contributions of the transversal (black) and longitudinal (red) mode to the overall extinction spectrum dependent on the polarizer angle with least-squares $\cos^2 \theta$ fit.

To obtain more quantitative information, extinction spectra were measured at various intermediate polarization angles, as shown in Figure 3a. The spectra measured between 30° and 120° showed contributions from both transversal and longitudinal modes and were interpreted as linear combinations of the two Lorentzian functions shown in Figure 3b. As the angle increased from 30° to 120°, the contribution from the longitudinal plasmon mode decreased whereas the contribution from the transversal plasmon mode increased, as indicated by the presence of a single isosbestic point at 729 nm. Figure 3b shows the relative contribution of the transversal (black) and longitudinal (red) plasmon extinction to the overall extinction spectra as function of the excitation polarization angle. A $\cos^2$ curve fit to these data indicated reproducible polarization-dependent behaviour of nanorod domain extinction intensity. The low intensity measured perpendicularly to the nanorod long axes corresponded to a max intensity along the direction of the nanorod long axes, indicating an almost perfect alignment of individual nanorods within the domain.

Further investigation by correlated polarized optical microscopy and electron microscopy revealed that small changes in the arrangement of nanorods within a domain resulted in large changes of the domain's optical features. For example, a color transition from red to pale green was observed in domains where nanorods were only loosely packed into side-by-side configuration, see Figure SI9. A corresponding transition from 735 nm to 580 nm was observed in the spectra recorded under polarized light oriented parallel and perpendicular to the nanorod long axes, respectively. These results hold potential for application of these superstructures as polarization-controlled colorimetric nanomaterials.

The organization of Au nanorods into domains and the arrangement of domains is determined by the balance of Van der Waals forces, capillary forces, surface tension and others operating during the evaporation process. Consequently, the droplet evaporation and stamping method allowed control on domain size and internal order but did not allow control on the final orientation of domains. This feature was applied to the development of a novel class of unique plasmonic identifiers. Figure 4a-c show polarized optical images of domains stamped on glass coverslips in areas of 900 μm^2, defined by focused ion beam (FIB) milled marks. Due to the high degree of internal order each domain was characterized by a distinct color. In addition, due to the random orientation of domains, each image displayed a unique distribution of color intensity patterns. To express this uniqueness numerically, optical images a-c were analyzed with common image analysis software (Image J). Each image was split into its individual RGB color channels from which in turn intensity histograms were extracted. The unique domain pattern (and coloring) resulted in distinctive histograms for each image, as shown in Figure 4d. The histograms of the green values were chosen since they showed the highest degree of diversity.
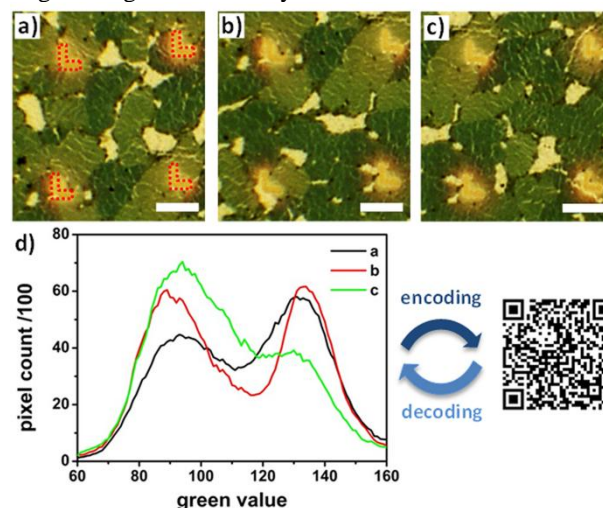

Figure 4. a-c) Polarized light transmission images of Au nanorod domains with 30×30 μm areas defined by FIB milled alignment marks highlighted in a) (scale bar 10 μm); d) Green value histograms calculated from images a-c by image J software. The displayed QR code contains the information of histogram a.

By converting intensity coordinates into text strings unique QR codes were created for each optical image.[33] As an example, the QR code displayed in Figure 4d corresponds to the area framed in figure a. As a verification tool, when this QR code was scanned by a QR code reading system, it generated the original text string which in turn could be converted into the original histogram by a MATLAB code containing the decoding information (for more details see Figure SI10).[34] Based on these findings, the formation of unique patterns that can be incorporated on transparent substrates could constitute the basis

for a novel plasmonic encoding system for anti-counterfeit applications.

In our proposed concept FIB milled alignment marks ensured that histograms could be repeatedly taken from precisely the same area on a tag. An additional level of complexity to the encryption could be added by using larger areas containing multiple frames. This way the encoded data could be a mathematical function of the histograms of specific squares. Implementing these substrates as anti-counterfeit tags would require a calibrated reader to ensure a reproducible optical read out of the tags. However, we believe the data shown here serves as prove of concept for this application.

The proposed variation of the droplet evaporation method produces uniform monolayer assemblies with a high degree of internal order. By suppression of the coffee stain mechanism, the method combines the low cost and simplicity of the droplet evaporation technique with the high output of more cumbersome techniques such as capillary or convective assembly.

One advantage of having high order in relatively large area domains is that the system acquires optical and electronic properties which are consistent and reproducible across the entire domain. This is advantageous for the proposed plasmonic anticouterfeiting application but also for optoelectronic and sensing applications, which are currently being explored by the authors.[35,36]

Conclusions

In conclusion, we have demonstrated the formation of Au nanorods superstructures by a combination of droplet evaporation and stamping technique. Nanorods assembled side-to-side into monolayer domains with an average size of 200 μm2. Optical characterization revealed a marked optical anisotropic behavior, confirming that nanorods were aligned within individual domains with a high degree of internal order. The unique orientation of domains, resulting in unique distribution of colors, was used for initial demonstration of plasmonic encoding/decoding systems for anti-counterfeit applications. We believe that the observed strong orientation of optical features may also allow for the development of novel orientation sensors and switchable displays. Moreover, the proposed fabrication method constitutes an excellent example of control over the long range ordering of Au nanorods that could be used as platforms for enhanced optical sensing applications.

Acknowledgements

Notes and references

[a] Tyndall national Institute, Dyke Parade, Cork, Ireland. E-mail: daniela.iacopino@tyndall.ie

Electronic Supplementary Information (ESI) available: [details of any supplementary information available should be included here]. See DOI: 10.1039/b000000x/

1   M. A. El-Sayed, *Acc. Chem. Res.,* 2001, **34**, 257-264.

2   M. C. Daniel and D. Astruc, *Chem. Rev.,* 2004, **104**, 293-346.

3   S. Link and M. A. El-Sayed, *J. Phys. Chem. B*, 1999, **103**, 8410-8426.

4   J. Perez-Juste, I. Pastoriza-Santos, L.M. Liz-Marzán and P. Mulvaney, *Coord. Chem. Rev*., 2005, **249**, 1870-1901.

5   R. Zia, J.A. Schuller, A. Chandran and M.L. Brongesma, *Mater. Today*, 2006, **9**, 20.

6   K.B. Crozier, A. Sundaramurthy, G.S. Kino and C.F. Quate, *J. Appl. Phys*., 2003, **94**, 4632-4642.

7   S. Eustis and M. El-Sayed, *J. Phys, Chem. B,* 2005, **109**, 16350-16356.

8   J. Kumar and K.G. Thomas, *J. Phys. Chem. Lett.,* 2011, **2**, 610-615.

9   D. Baranov, L. Manna and A.G. Karanas, *J. Mater. Chem*., 2011, **21**, 16694-16703.

10   M.R. Jones, K.D. Osberg, R.J. Macfarlane, M.R. Langille and C.A. Mirkin, *Chem. Soc. Rev.,* 2011, **111**, 3736-3827.

11   Z.H. Nie, A. Petukhova and E. Kumacheva, *Nat. Nanotech.*, 2010, **5**, 15-25.

12   M. Zanella, R. Gomes, M. Povia, C. Giannini, Y. Zhang, A. Riskin, M. Van Bael, Z. Hens and L. Manna, *Adv. Mater.,* 2011, **23**, 2205-2209

13   C.J. Murphy, T.K. Sau, A. M. Gole, C.J. Orendoff, J. Gao, L. Gou, S.E. Hunyandi and T. Li, *J. Phys. Chem. B*, 2005, **109**, 13857-13870.

14   C. Kuemin, L. Novack, L. Boano, N. D. Spencer and H. Wolf, *Adv. Funct. Mater.*, 2012, **22**, 702-708.

15   M. Sethi, G. Joung and M.R. Knecht, *Langmuir*, 2009, **25**, 1572-1581

16   T.S. Sreprasad, A.K. Samal and T. Pradeep, *Langmuir*, 2008, **24**, 4589-4599.

17   H. Natashima, K. Furukawa, Y. Kashimura and K. Torimitsu, *Langmuir,* 2008, **24**, 5654-5658.

18   T.K. Sau and C.J. Murphy, *Langmuir,* 2005, **21**, 2923-2929

19   D. Nepal, M.S. Onses, K. Park, M. Jespersen, C.J. Thode, P.F. Nealey and R.A. Vaia, *ACS Nano*, 2012, **6 (6)**, 5693–5701.

20   T, Ming, X. Kou, H. Chen, T. Wang, H-L. Tam, K-W. Ceah, J-Y. Chen and J. Wang, *Angew. Chem Int. Ed.,* 2008, **120**, 9831-9836.

21   Y. Xie, S. Guo, C. Guo, M. He, D. Chen, Y. Ji, Z. Chen, X. Wu, Q. Liu and S. Xie, *Langmuir*, 2013, **29**, 6232-6241.

22   B. Peng, G. Li, D. Li, S. Dodson, Q. Zhang, J. Zhang, Y. H. Lee, H. V. Demir, X. Y. Ling and Q. Xion, *ACS Nano*, 2013, **7**, 5993-6000.

23   B. Nikoobakht and M. A. El-Sayed, *Chem. Mater*., 2003, **15,** 1957-1962

24   J. Yang, J-C. Wu, J-K. Wang and C-C. Chen, *Chem. Phys. Lett*., 2005, **416**, 215-219.

25   K. Weidemaier, H.L. Tavernier and M.D Fayer, *J. Phys. Chem. B*, 1997, **101**, 9352-9361.

26   H. Nakashima, K. Furukawa, Y. Kashimura, K. Torimitsu Langmuir, 2008, 24, 5654-5658.

27   Z. Zhu, H. Meng, W. Liu, X. Liu, J. Gong, X. Qiu, L. Jiang, D. Wang, Z. Tang *Angew. Chem Intern. Ed.,* 2011, **50**, 1593-1596).

28   T. K. Sau, C. J. Murphy *Langmuir*, 2005, **21**, 2923-2929.

29   Q. Ji, S. Acharya, J. P. Hill, G. J. Richards, K. Ariga *Adv. Mater.* 2008, **20**, 4027-4032.

30   Y. Huang, D. –H. Kim *Langmuir*, 2011, **27**, 13861-13867.

31   P.K. Jain, S. Eustis and M. El-Sayed J. *Phys. Chem. B*, 2006, **110**, 18243-18253.

32   Y. Huang, D. –H. Kim *Nanoscale*, 2011, **3**, 3228-3232.

33   http://qrcodemakr.com

34   htpp:// online-barcode-reader.inliteresearch.com

35 A. Martín, A. Pescaglini, C.schopf, V. Scardaci, R. Coull, L. Byrne, D. Iacopino, J. Phys. Chem. C, 2013, submitted.

36 S. Diefenbach, N. Erhard, J. Schopka, A. Martin, C. Karnetzky, D. Iacopino, A. W. Holleitner Phisica Status Solidi, 2014, DOI 10.1002/pssr.201308305.